

- [9] H. Fujisawa, K. Morimoto, M. Shimizu, H. Niu, K. Honda, S. Ohtani, *Mater. Res. Soc. Symp. Proc.* **2001**, 655, CC10.4.1.
- [10] W. Ma, D. Hesse, *Appl. Phys. Lett.* **2004**, 84, 2871.
- [11] R. Waser, T. Schneller, S. Hoffmann-Eifert, P. Ehrhart, *Integr. Ferroelectr.* **2001**, 36, 3.
- [12] R. W. Schwartz, T. Schneller, R. Waser, *C. R. Chimie* **2004**, 7, 433.
- [13] A. Seifert, A. Vojta, J. S. Speck, F. F. Lange, *J. Mater. Res.* **1996**, 11, 1470.
- [14] A. Roelofs, T. Schneller, K. Szot, R. Waser, *Appl. Phys. Lett.* **2002**, 81, 5231.
- [15] A. Rüdiger, T. Schneller, A. Roelofs, S. Tiedke, T. Schmitz, R. Waser, *Appl. Phys. A: Mater. Sci. Process* **2005**, 80, 1247.
- [16] M. Dawber, I. Szafraniak, M. Alexe, J. F. Scott, *J. Phys.: Condens. Matter* **2003**, 15, L667.
- [17] T. Schneller, R. Waser, *Ferroelectrics* **2002**, 267, 293.
- [18] P. Muralt, T. Maeder, L. Sagalowicz, S. Hiboux, *J. Appl. Phys.* **1998**, 83, 3835.
- [19] R. Bouregba, G. Poullain, B. Vilquin, H. Murray, *Mater. Res. Bull.* **2000**, 35, 1381.
- [20] S. Bühlmann, P. Muralt, S. Von Allmen, *Appl. Phys. Lett.* **2004**, 84, 2614.
- [21] A. Beck, J. G. Bednorz, Ch. Gerber, C. Rossel, D. Widmer, *Appl. Phys. Lett.* **2000**, 77, 139.
- [22] D. W. Carr, R. C. Tiberio, *Mater. Res. Soc. Symp. Proc.* **2000**, 584, 305.
- [23] It was noted that the titanium layer converts into titanium oxide (TiO₂) due to contact with oxygen from the environment, especially because of the small layer thickness.
- [24] R. Nouwen, J. Mullens, D. Franco, J. Yperman, L. C. Van Poucke, *Vib. Spectrosc.* **1996**, 10, 291.
- [25] D. J. Wouters, G. J. Norga, H. E. Maes, *Mater. Res. Soc. Symp. Proc.* **1999**, 541, 381.
- [26] I. Szafraniak, C. Harnagea, R. Scholz, S. Bhattacharyya, D. Hesse, M. Alexe, *Appl. Phys. Lett.* **2003**, 83, 2211.
- [27] Supplied by Allresist (Strausberg, Germany).

Cutting into Solids with Micropatterned Gels**

By Stoyan K. Smoukov, Kyle J. M. Bishop, Rafal Klajn, Christopher J. Campbell, and Bartosz A. Grzybowski*

The ability to microstructure solid surfaces, that is, to modify their microscale topographies, is important in several modern technologies, including microfluidics,^[1,2] optoelec-

tronics,^[3] and water-repellent surfaces.^[4,5] Existing microstructuring methods are either serial in nature and/or expensive (X-ray lithography,^[6] micromachining,^[7] laser etching,^[8] reactive ion etching (RIE)^[9]) or rely on protective coatings^{[10]/micromembranes,^[11] which often delaminate or get under-etched. We have previously suggested^[12,13] that microscale reaction–diffusion processes in two-phase systems can provide a basis for new microfabrication and structure-modification techniques. In particular, we have shown that micropatterned hydrogel stamps can be used to deliver chemicals controllably—by diffusive processes enhanced by osmotic pressure gradients^[14]—into thin films of dry gels and initiate a variety of chemical processes (e.g., swelling,^[15,16] periodic precipitation,^[17] oscillating reactions^[18]) therein. Here, we demonstrate that such stamps can also be used to remove material from solid surfaces and can thus be used to microstructure metals, glasses, and crystals with micrometer-scale precision. In our system, the gel stamp provides a reservoir of an etching/dissolving chemical, which reacts with the solid support at the top of the stamp's microfeatures; at the same time, the products of one or more reactions occurring at the interface between the phases are cleared by diffusive transport into the gel's bulk. Overall, the stamp cuts into the solid along the micropattern embossed on its surface and microstructures this solid with high-aspect-ratio and/or quasi-three-dimensional (quasi-3D) microfeatures.}

Hydrogel stamps were made according to the procedure described in detail before^[12,13] and outlined in the Experimental section. To microstructure metals (Fig. 1), the stamps were soaked in a solution of an appropriate commercial etchant (for Au, 25 % water solution of TFA etchant, Transene Company, Danvers, MA; for Cu and Ni, 35 % water solution of FeCl₃-based PCB RadioShack etchant, cat. no. 276-1535; for Fe, HNO₃ 5–10 % in water) for 2 h, and applied onto a metal surface. For thin, thermally evaporated layers of metal (10 nm Ti adhesion layer and ~100 nm Ni or Au, Fig. 1b), the area below the features of the stamp was completely etched within ~1 s from the application of the stamp, and the etched pattern was a faithful copy of the pattern in the stamp with resolution down to ~2 μm (Fig. 1b, right). For longer application times, the etchant could either reactively spread^[19] on the surface or remain contained in the features. This depended on the properties of the material below the metal: for hydrophilic surfaces (e.g., glass), spreading occurred at a rate of several micrometers per minute; for hydrophobic ones (e.g., polystyrene) it was negligible. We note that unlike other microetching methods, which require patterning of a metal substrate with a protective monolayer prior to etching, wet stamping (WETS) leaves behind a clean metal surface that can be chemically derivatized *after* etching.

Because the stamps carried large amounts of the etching solution, they could cut deep into thick metal supports. Figure 1c shows microstructures etched in a 50 μm thick copper foil. The picture on the left has 30 μm tall star posts obtained

[*] Prof. B. A. Grzybowski, Dr. S. K. Smoukov, K. J. M. Bishop, R. Klajn, C. J. Campbell
Department of Chemical Engineering and
The Northwestern Institute on Complex Systems
Northwestern University
2145 Sheridan Road, Evanston, IL 60208 (USA)
E-mail: grzybor@northwestern.edu

[**] B.G. gratefully acknowledges financial support from Northwestern University start-up funds and from the Camille and Henry Dreyfus New Faculty Awards Program. K.B. and C.C. were supported in part by the NSF-IGERT program "Dynamics of Complex Systems in Science and Engineering" (DGE-9987577).

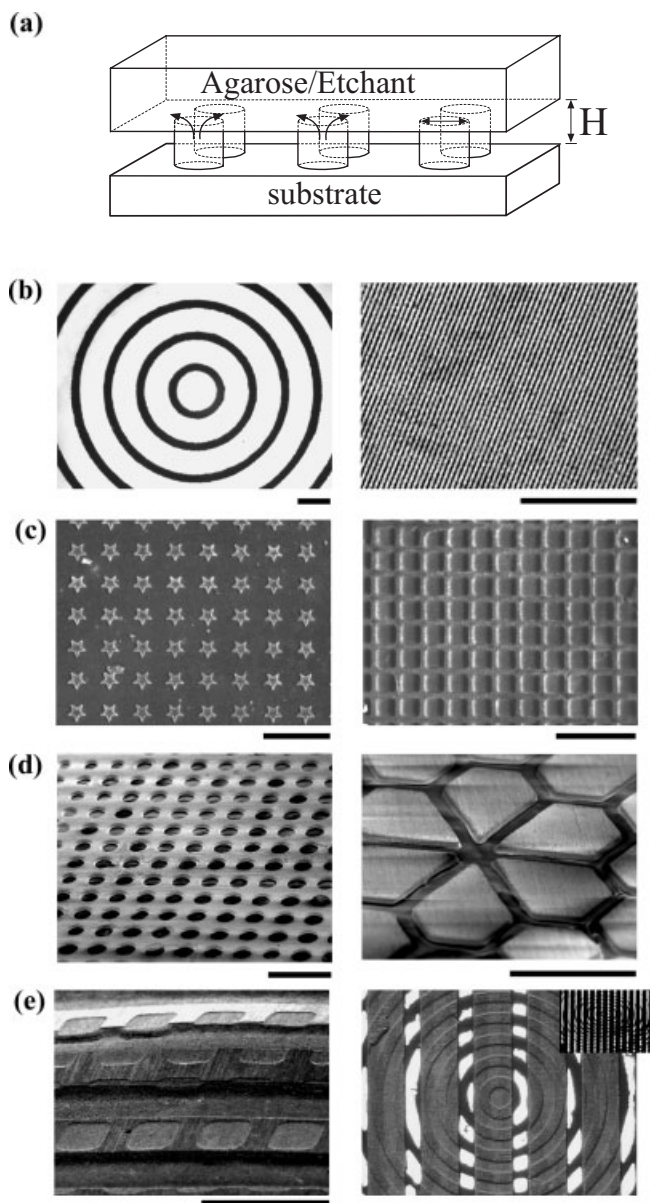


Figure 1. Etching of metal supports using wet stamping (WETS). a) Scheme of the experimental arrangement. b) Patterns etched in 100 nm thick, thermally evaporated layers of Ni (left) and Au (right); pattern on the right is an array of 1.5 μm lines spaced by 2.5 μm . Scale bars, 50 μm . c) Posts and wells etched in a copper foil. d) Membranes and metal plates obtained from the same foil for long (here, 8 h) etching times. e) Quasi-3D structures obtained by consecutive stamping of two different patterns. Left: An array of deeper, parallel lines ($\sim 35 \mu\text{m}$) was etched into a foil that had already been patterned with a shallower ($\sim 8 \mu\text{m}$) array of squares. Right: A pattern of concentric circles $\sim 10 \mu\text{m}$ deep was first etched into a copper film, followed by etching of an array of parallel lines using a stamp made out of a softer agarose ($\sim 7 \text{ wt.-%}$) that conformed to the shape of the patterned surface. In the regions where the circles had been etched, the lines cut all the way through the film; in other locations, $\sim 10 \mu\text{m}$ thick circular metal “ribs” remained at the bottom of the foil. Aside from its complex topography, the pattern is interesting for the visual illusion (moiré pattern) it creates, shown in the inset, in which the circles appear to be ellipses. Scale bars correspond throughout to 500 μm unless otherwise stated.

from a stamp with corresponding star wells, while that on the right shows square wells prepared using a stamp with square posts in bas relief. In both cases, the stamps were placed on the foil for 3 h. For longer etching times, the stamps cut through the entire copper film to give either membranes (using stamps patterned with posts, Fig. 1d, left) or disjointed metal plates (when stamps had a network of connected features in bas relief, Fig. 1d, right). With consecutive stampings using the same or different patterns, we were able to prepare multilevel microstructures such as those illustrated in Figure 1e. The maximum depth of etched features was $\sim 100 \mu\text{m}$ with aspect ratios as high as 2; all types of structures had excellent uniformity over areas up to 1 cm^2 . We briefly mention that, in general, stamps could be reused for up to $\sim 8 \text{ h}$; for longer times, the acidic etchants caused softening of the agarose matrix.

Vertical “sinking” of the stamps into metal substrates was accompanied by only minimal horizontal etching (not more than ca. $\sim 6 \%$ of the feature size). Because the surface layer of liquid was removed from the stamp’s surface prior to patterning, and because the water-based etchant did not wet the metal surface, it was tightly confined to the stamp’s features by hydration forces. Consequently, after some initial etching at the sides of the features, these sides lost contact with the substrate; etching continued only at the interface between the tops of the features and the bottoms of the indentations in the metal.

The depth of the etched features H increased monotonically with time t . The experimentally observed dependence shown in Figure 2c is explained by a model that assumes that the etching rate is proportional to the flux of etchant at the metal–stamp interface, and that the etching reaction occurs much faster than the diffusion of the etchant within the stamp (i.e., it is diffusion limited). For a model geometry of a stamp patterned with an array of small cylindrical features of radius R and height L , the pertinent diffusion equation can be solved analytically by first solving piecewise over the regions of the feature and of the stamp “reservoir,” and then connecting the solutions using equality of concentrations and fluxes at the boundary between the two regions.

Assuming that the concentration of the etchant in the stamp is i) uniform before stamping, $C(x,0) = C_0$, ii) fixed at zero at the stamp–metal interface, $C(0,t) = 0$, and iii) remains unchanged far from the interface, $C(\infty,t) = C_0$, the rate of etching can be expressed as

$$dH/dt = -aDC^*(t)/L \left[1 + 2 \sum_{n=1}^{\infty} \exp(-Dn^2\pi^2 t/L^2) \right] \quad (1)$$

where a is a constant of proportionality, D is the diffusion coefficient of the etchant in the stamp, and $C(t)$ is the concentration at the feature–reservoir interface (see Experimental section). This function can be simplified in the limits of “short” ($\tau = L^2/D \ll 1$) and “long” ($\tau \geq 1$) times. Short times

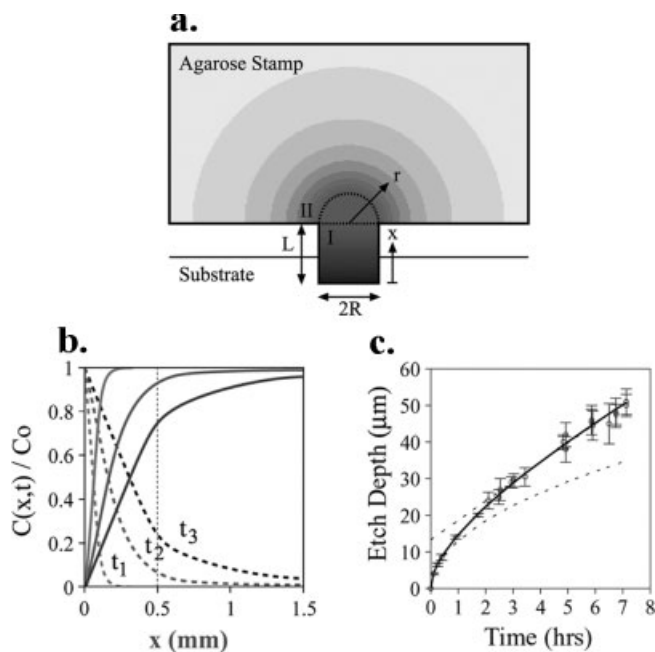


Figure 2. Calculated concentration profiles and etching rates. a) Scheme of a large stamp “reservoir” with a cylindrical feature cutting into a solid support. Isoconcentration profiles, colored in shades of gray, were calculated using the two-region analytical matching method for $L = 500 \mu\text{m}$, $R = 250 \mu\text{m}$, and $\tau = L^2/D = 1$. b) Concentration profiles along the axis of a cylindrical feature extending into the stamp reservoir (zero position corresponds to the stamp–substrate interface; the dashed vertical line delineates the interface between the feature and the reservoir, $x = L$). Times t_1 , t_2 , and t_3 correspond to $\tau = L^2/D = 0.01$, 0.1 , and 1 , respectively. Solid curves represent concentration profiles for a process in which an etchant is consumed by reaction at $x = 0$ (e.g., etching metals). Dashed lines have the profiles of a solute, which is continuously dissolved at the stamp–substrate interface and transported into the stamp’s bulk (e.g., etching crystals). Note that for $\tau = 1$ the profiles are linear in the feature. In this regime, the reservoir continuously delivers/removes the solute, and the etching rate approaches a constant value. c) Dependence of the depth of the etched features, H , on the time of stamp application. The values of H were measured by profilometry; error bars correspond to standard deviations based on at least three independent stampings of an array of $100 \mu\text{m}$ circles for each value of time. In all cases, concentration of the FeCl_3 -based etchant in the stamp was 18%. The solid line is a theoretical fit based on the analytical, two-region solution. The dashed lines are the fits for the limits of short times (square-root dependence) and long times (linear dependence).

are dominated by diffusion in the features, and the etching rate is given by

$$dH/dt = aC_0\sqrt{D/\pi t} \quad (2)$$

At long times delivery from the reservoir dominates, and

$$dH/dt = DC_0/(L + R/2) \quad (3)$$

In other words, at short times, the depth of the etched wells increases as the square root of time while for long times it grows linearly with t . These predictions are in excellent agreement with experiment (Fig. 2c).

If the solutions contained in the stamps wetted the surfaces of the substrates (e.g., HF on glass, water on ionic crystals), the quality of etching in air was poor and led to surface indentations that had blunt edges and were significantly larger than the stamped features. These problems were eliminated by immersion (or under-liquid) wet stamping (i-WETS).

For example, to microstructure glass, agarose stamps were soaked in a solution of 2% w/v HF, up to 16.7% (v/v) HCl (to increase the etching rate^[20]) and 0.5% Triton X-100 surfactant (MP Biomedicals, CAS# 9002-93-1), which improved the smoothness of the etched surfaces. After drying of the gel’s surface, the stamp was placed upside down at the bottom of a dish filled with mineral oil (Light Mineral Oil, 0121-1, Fisher Scientific) immiscible with the etching solution (Fig. 3a). A glass substrate was then placed on the stamp and came into conformal contact with the tops of the stamp’s features. At the same time, the grooves between the features remained filled with oil, thus preventing spreading of the etching solution onto the glass surface. As the stamp etched into the substrate, oil also filled the gap that formed—as a result of initial horizontal etching (<6% of the feature size)—between the sides of the features and sides of the carved wells. This thin oil layer protected the glass from further etching, which continued only at the tops of the features and cleanly in the vertical direction. The carved-out depressions (Figs. 3b–d) had sharp edges, and their maximum depth (limited only by the depth of the features in the stamps we used) was $\sim 70 \mu\text{m}$,^[21] significantly larger than that achievable by other parallel etching techniques.

The i-WETS technique proved equally successful in microstructuring surfaces of monocrystals (Figs. 3e–f) with depths of the depressions up to $80 \mu\text{m}$, sharp edges, and lateral spreading less than 5% of the diameter of the stamped features. We were able to microstructure both inorganic (e.g., calcium carbonate, potassium hexacyanoferrate) and organic (e.g., sucrose, naphthalene) crystals. We note that for crystals readily soluble in water (e.g., $\text{K}_3\text{Fe}(\text{CN})_6$), the best results were obtained with stamps soaked in mixtures of water and ethanol (5:95 v/v). Pure-water stamps etched into crystals too rapidly and with pronounced lateral spreading. An ethanol base for the “etchant” made the process more controllable, and also reduced surface tension with respect to the oil, which could thus penetrate into the side regions of the etched wells more easily. Based on these and the preceding results for metals and glass, we suggest that the rule of using low-concentration solutions of an etchant can be generalized to other substrates.

Finally, we remark that non-binary surface topographies can be achieved by engineering diffusive fluxes *in* the stamps and coupling these fluxes to chemical reactions involving dissolved substrates. This is vividly illustrated in the inset to Figure 3f, which shows “toroidal” depressions etched by a stamp soaked in a solution of 0.5 M FeSO_4 and patterned with an array of circles onto a crystal of $\text{K}_3\text{Fe}(\text{CN})_6$. Briefly, as the dissolved hexacyanoferrate ions from the crystal diffuse into the stamp, they are instantaneously precipitated in a reaction with

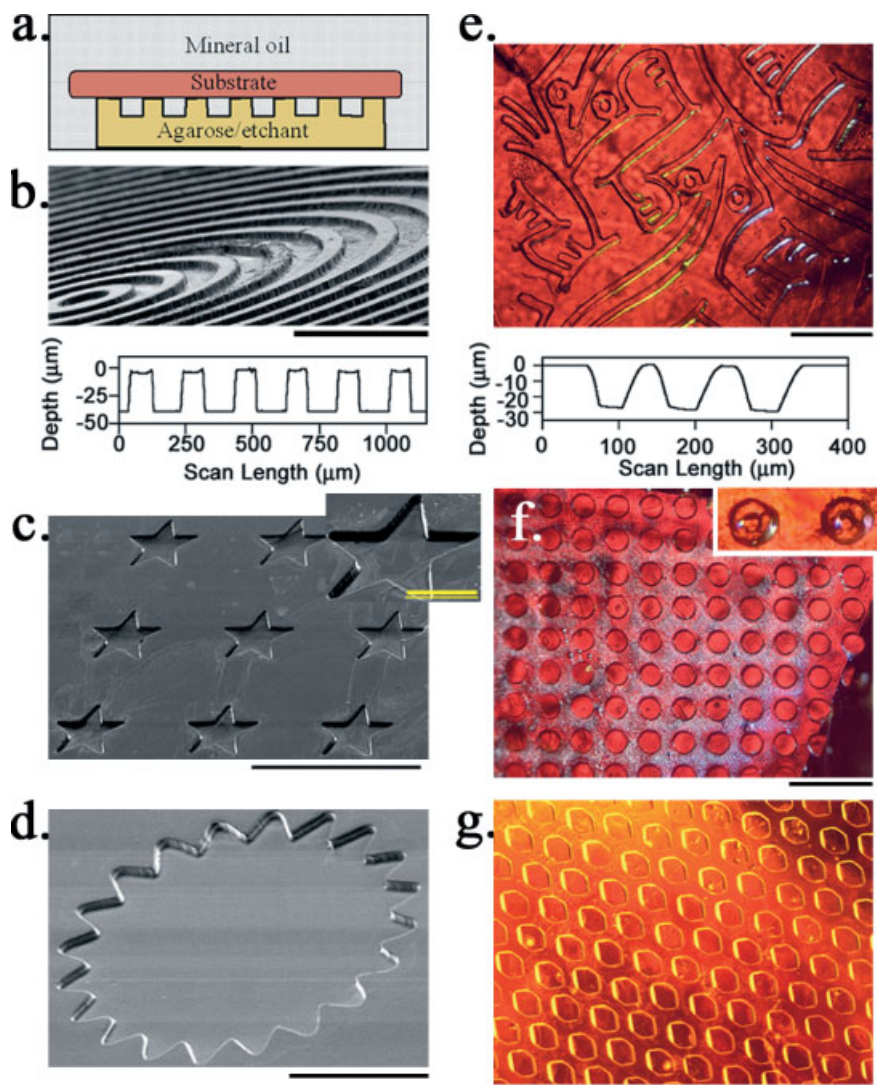


Figure 3. Microstructuring of glass and crystals with i-WETS. a) Scheme of the i-WETS procedure. b) Array of concentric circles etched in glass; the corresponding profilogram along the circles' diagonals is shown below (scale bar, 500 μm). c) SEM image of a pentagonal star etched in glass (scale bar, 500 μm), with inset highlighting well-resolved edges and points (scale bar, 100 μm). d) Twenty-spoked gear etched into glass (scale bar, 250 μm). e) Escher's lizards microstructured into crystals of $\text{K}_3\text{Fe}(\text{CN})_6$ (scale bar, 500 μm). Profilogram taken across the three splayed lizard "fingers" near the top left of the photograph. f) Circles, 50 μm diameter, etched into a crystal of $\text{K}_3\text{Fe}(\text{CN})_6$ (scale bar, 200 μm). The inset shows that etching with a 0.5 M solution of FeSO_4 gives torus-shaped depressions with centers ~ 30 μm less deep than the edge regions (~ 80 μm deep). g) Array of 30 μm deep hexagons etched (15 min) into the face of a calcium carbonate (calcite) crystal using stamps soaked in 1.2 M HCl.

iron(II) cations contained therein: $\text{Fe}^{2+} + [\text{Fe}^{\text{III}}(\text{CN})_6]^{3-} + \text{K}^+ \rightarrow \text{KFe}^{\text{II}}[\text{Fe}^{\text{III}}(\text{CN})_6]$ (\downarrow). Because diffusive fluxes are highest near the edges of the features,^[22] these regions serve as sinks of both Fe^{2+} from the stamp and $[\text{Fe}^{\text{III}}(\text{CN})_6]^{3-}$ from the crystal. In particular, unreacted iron(II) cations contained in the stamp migrate from the features' centers towards the edges, where they "scavenge" the dissolved anions from the crystal. As a result, etching proceeds more rapidly at the regions near the edges, and the etched depressions are deeper around the contours of the features and shallower near their centers. A

mathematical description of the complex interplay^[22] between reaction, diffusion, surface wetting, and feature geometry in this system will be the subject of a separate communication.

In summary, we have described a simple, versatile, and reliable method of microstructuring solid supports. We believe that WETS and i-WETS techniques will prove useful in rapid prototyping of microfluidic circuits in glass, fabrication of metallic membranes and microstructured foils with applications in separation science and light-weight materials, and of optical elements (e.g., polarizing diffraction gratings from crystals). In specific applications, it might be necessary to use hydrogels other than agarose to make the stamps compatible with desirable etchants.

Experimental

Stamp Fabrication: A hot, degassed 8–12 % w/w solution of high strength agarose (OmniPur Agarose, Darmstadt, Germany) in deionized water was cast against an oxidized poly(dimethyl siloxane) (PDMS) master that had an array of microscopic features embossed on its surface (typical feature size, $2 \mu\text{m} \leq W \leq 250 \mu\text{m}$, feature depth, $2 \mu\text{m} \leq H \leq 100 \mu\text{m}$, $0.4 \leq H/W \leq 2$). After further degassing under vacuum and gelation, the agarose layer was gently peeled off and cut into approximately 1–2 cm \times 1–2 cm \times 2–5 mm rectangular blocks ("stamps") patterned with the negative of the array of features in the PDMS master. Next, the stamps were soaked for 10–120 min in an aqueous solution of a reagent to be used in surface microstructuring (see below). Immediately prior to use, the stamps were dried of excess water by blowing dry nitrogen over them (~ 30 s) and then placing on a filter paper for 20 min. Finally, the stamps were put onto a glass slide for 10 min (pattern side down) to equalize any hydration gradients that might have developed during drying.

Modeling: The diffusion equation in agarose stamps was solved piecewise for the features and for the stamp's bulk (the "reservoir"). Consider a cylindrical feature (region I) of height L and radius R much smaller than the dimensions of the attached reservoir (region II). The reservoir is approximated as a semi-infinite half-space bounded by the hemisphere of radius R "capping" the cylindrical feature (i.e., a region defined in spherical coordinates as $R < r < \infty$, $0 < \phi < \pi/2$, and $0 < \theta < 2\pi$). These regions were chosen to facilitate analytical approximation, which approaches an exact solution in the limit as $R/L \rightarrow 0$. Initially, the stamp has a uniform etchant concentration C_0 , and upon stamping, a "fast" etching reaction maintains a zero concentration at the stamp/substrate interface; the concentration at the interface between regions I and II is denoted as $C^*(t)$, and its value is determined by the solution matching process.

In region I, diffusion is described by the one-dimensional diffusion equation

$$\partial C_1(x, t) / \partial t = D \partial^2 C_1(x, t) / \partial x^2; 0 \leq x \leq L \quad (4)$$

The boundary conditions are $C_1(0, t) = 0$ at $x = 0$ and $C_1(L, t) = C^*(t)$ at $x = L$, and the initial condition is $C_1(x, 0) = C_0$. Because $C^*(t)$ decreases slowly, i.e.,

$$dC^*(t) / dt < DC_0 / L^2 \quad (5)$$

and monotonically, this problem is well approximated by the following series solution for unsteady diffusion between constant boundary concentrations:

$$C_1(x, t) = C^*(t) (x/L) + 2/\pi \sum_{n=1}^{\infty} ((-1)^n C^*(t) / n) \sin(n\pi x / L) \exp(-Dn^2 \pi^2 t / L^2) \quad (6)$$

where the time dependence of $C^*(t)$ has been inserted after the diffusion equation has been solved.

In region II, spherical symmetry leads to a diffusion equation in spherical coordinates

$$\partial C_{II}(r, t) / \partial t = D / r^2 \partial / \partial r (r^2 \partial C_{II}(r, t) / \partial r) \text{ for } R \leq r < \infty \quad (7)$$

The boundary conditions are $C_{II}(R, t) = C^*(t)$ at $r = R$ and $C_{II}(\infty, t) = C_0$ as $r \rightarrow \infty$, and the initial condition is $C_{II}(x, 0) = C_0$. This problem can be well approximated analytically to give

$$C(r, t) = C_0 - (C_0 - C^*(t)) (R/r) \operatorname{erfc}((r - R) / \sqrt{4Dt}) \quad (8)$$

where, again, the time dependence of $C^*(t)$ has been neglected until after the diffusion equation has been solved.

To determine the functional form of $C^*(t)$ it is necessary to equate the molar flow rates across the boundary between regions I and II

$$-D(\partial C_1 / \partial x)_L \pi R^2 = -D(\partial C_{II} / \partial r)_R 2\pi R^2 \quad (9)$$

Doing so allows one to find

$$C^*(t) = \frac{2C_0(1/R + 1/\sqrt{\pi Dt})}{2/R + 2/\sqrt{\pi Dt} + 1/L + 2/L \sum_{n=1}^{\infty} \exp(-Dn^2 \pi^2 t / L^2)} \quad (10)$$

To relate the concentration profiles to etching rates, it is assumed that the rate of etching is proportional to the flux at the stamp/substrate interface

$$dH/dt \propto -D(\partial C_1 / \partial x)_{x=0} \quad (11)$$

or

$$dH/dt = aDC^*(t) / L \left[1 + 2 \sum_{n=1}^{\infty} \exp(-Dn^2 \pi^2 t / L^2) \right] \quad (12)$$

In the limits of short and long times, this expression simplifies to the equations given in the text (Eqs. 2 and 3).

The procedure described above applies to etching of a substrate, in which the limiting process is the diffusion of the etchant from the stamp towards the surface. An analogous approach can be used to describe microstructuring of a crystal, in which the stamp continuously transports the solute from the crystal's surface into the reservoir. In this case, the solute concentration at the stamp/crystal interface is fixed at an equilibrium value determined by solubility. The concentration is initially zero throughout the stamp, and remains so far from the feature. This "inverse" problem can be solved by the change of

variables $C_{\text{inverse}} = C_0 - C$, where C is given by the solution derived above. This transformation of variables does not affect the expression for the etching rate but changes the sign of the proportionality constant a .

Received: December 21, 2004
Final version: January 11, 2005

- [1] A. D. Stroock, S. K. W. Dertinger, A. Ajdari, I. Mezic, H. A. Stone, G. M. Whitesides, *Science* **2002**, 295, 647.
- [2] H. A. Stone, A. D. Stroock, A. Ajdari, *Annu. Rev. Fluid Mech.* **2004**, 36, 381.
- [3] G. Steinmeyer, *J. Opt. A* **2003**, 5, R1.
- [4] H. Y. Erbil, A. L. Demirel, Y. Avci, O. Mert, *Science* **2003**, 299, 1377.
- [5] L. Feng, Y. L. Song, J. Zhai, B. Q. Liu, J. Xu, L. Jiang, D. B. Zhu, *Angew. Chem. Int. Ed.* **2003**, 42, 800.
- [6] E. W. Becker, W. Ehrfeld, P. Haggmann, A. Maner, D. Muenchmeyer, *Microelectron. Eng.* **1986**, 4, 35.
- [7] J. M. Bustillo, R. T. Howe, R. S. Muller, *Proc. IEEE* **1998**, 86, 1552.
- [8] D. J. Ehrlich, R. M. Osgood, T. F. Deutsch, *Appl. Phys. Lett.* **1981**, 38, 1018.
- [9] L. M. Ephrath, *J. Electrochem. Soc.* **1979**, 126, 1419.
- [10] Y. N. Xia, X. M. Zhao, E. Kim, G. M. Whitesides, *Chem. Mater.* **1995**, 7, 2332.
- [11] R. J. Jackman, D. C. Duffy, O. Cherniavskaya, G. M. Whitesides, *Langmuir* **1999**, 15, 2973.
- [12] C. J. Campbell, M. Fialkowski, R. Klajn, I. T. Bensemann, B. A. Grzybowski, *Adv. Mater.* **2004**, 16, 1912.
- [13] R. Klajn, M. Fialkowski, I. T. Bensemann, A. Bitner, C. J. Campbell, K. Bishop, S. Smoukov, B. A. Grzybowski, *Nat. Mater.* **2004**, 3, 729.
- [14] M. Fialkowski, C. J. Campbell, I. T. Bensemann, B. A. Grzybowski, *Langmuir* **2004**, 20, 3513.
- [15] C. J. Campbell, R. Klajn, M. Fialkowski, B. A. Grzybowski, *Langmuir* **2005**, 21, 418.
- [16] C. J. Campbell, E. Baker, M. Fialkowski, B. A. Grzybowski, *Appl. Phys. Lett.* **2004**, 85, 1871.
- [17] I. T. Bensemann, M. Fialkowski, B. A. Grzybowski, *J. Phys. Chem. B* **2004**, 109, 2774.
- [18] K. J. M. Bishop, B. A. Grzybowski, unpublished.
- [19] Y. N. Xia, G. M. Whitesides, *J. Am. Chem. Soc.* **1995**, 117, 3274.
- [20] S. Verhaverbeke, I. Teerlinck, C. Vinckier, G. Stevens, R. Cartuyvels, M. M. Heyns, *J. Electrochem. Soc.* **1994**, 141, 2852.
- [21] A. R. Kopf-Sill, J. W. Parce, *US Patent 6517234*, **2003**.
- [22] S. K. Smoukov, K. J. M. Bishop, C. J. Campbell, B. A. Grzybowski, *Adv. Mater.* **2005**, 17, 751.